Capillary cohesion and mechanical strength of polydisperse granular materials

Fabien Soulié, Moulay Saïd El Youssoufi, Fabien Cherblanc, Christian Saix

Capillary cohesion and mechanical strength of polydisperse granular materials

F. Soulié[a], M.S. El Youssoufi, F. Cherblanc, and C. Saix

LMGC, UMR 5508 Université Montpellier 2, cc048 Place Eugène Bataillon, 34095 Montpellier Cedex 5, France

Abstract. We investigate the macroscopic mechanical behaviour of wet polydisperse granular media. Cap-illary bonding between two grains of unequal diameters is described by a realistic force law implemented in a molecular-dynamics algorithm together with a protocol for the distribution of water in the bulk. Axial-compression tests are simulated for granular samples at different levels of water content, and compared to experiments performed in similar conditions. We find good agreement between numerical and experimental data in terms of the rupture strength as a function of water content. Our results show the importance of the distribution of water for the mechanical behaviour.

1 Introduction

Small amount of water added to a granular mass has a strong effect on its mechanical behaviour. That is how sandcastles made from wet-sand grains keep standing [1,2]. It can be shown that for 2 mm-sized sand grains, the capillary force acting between grains is of the same order of magnitude as a single grain weight. This force is strong enough to allow a granular mass to maintain its proper shape in the gravity field. The effect of capillary forces is of special interest to many fields including unsaturated soil mechanics and process industries (mineral, agronomic, chemicals and pharmaceuticals) [3–5].

The mechanical behaviour of wet granular materials has been investigated both by experiments and numerical simulations. Several experimental studies have focused on the influence of gravimetric water content w on the mechanical strength. In granulation processes, it has been observed that loose agglomerates are consolidated by increasing the moisture content [6]. The tensile strength [7,8] and crushing strength [9] have also been studied as a function of water content. All these studies, concerning for the most part the powder industry, have been carried out for particles with diameters ranging from a few tens to a few hundreds of microns. In fact, the agglomerate resistance is inversely proportional to the particle size. Small grains are thus more adapted for the measurement of capillary force. A major issue is that local information at the particle scale is hardly accessible by experiments.

[a] e-mail: soulie@lmgc.univ-montp2.fr

There is a class of models dealing with wet granular materials directly at the scale of a representative elementary volume (REV). Such models are often used in the framework of finite-element simulations. The scope of this approach is limited to particular applications. In fact, such models involve phenomenological parameters bearing no direct relation with the local interactions or the microstructure. In some cases, such as fracture initiation and propagation, the particle interactions play an important role and it is desirable to be able to account *ab initio* for the local physics. This particle scale modeling, known as discrete element method (DEM), provides a powerful tool for the investigation of granular media. It has been applied to wet granular materials only recently; see, *e.g.*, [10,11]. Simulations using interactions of capillary type between grains have also been used to study aggregate formation in fluidized beds [12] or sheared granular materials [13].

Many reported DEM simulations deal with monodisperse packings and there is an extensive literature dealing with capillary forces for grains of equal diameters [14–16,7,12,17]. Most real granular materials, such as soils, involve, however, a more or less broad distribution of grain diameters. As we shall see below, capillary forces are strongly dependent on grains diameters. It is thus essential to account properly for polydispersity (particle size distribution) in view of application to real materials.

Another important issue concerns the distribution of water inside the granular packing. The capillary forces appear for low water contents in the form of "bridges" between grains. In this "pendular" state, the spatial distribution of liquid bridges is not well known. Recent

microscopic observations provide interesting information about the evolution of the number of mobilized liquid bridges as a function of water content and the compactness in the case of monodisperse packings [18,19]. However, the number of liquid bridges is dependent on the polydispersity and the anisotropy of granular arrangement.

Because of the limitations of the experimental approach and the complexity at the local scale (steric exclusions, capillary forces, polydispersity, distribution of capillary bonds), a multiscale approach bringing together modeling, DEM simulations and experiments is necessary. Indeed, experimental and numerical studies, carried out under similar conditions of granularity, compactness, anisotropy and water contents, should provide new insights by checking for the consistency of the data and the relevance of various modeling choices.

In this paper, we propose three complementary studies of wet granular media:

- Modeling of local interactions with experimental validation at this scale.
- Three-dimensional DEM simulations of polydisperse packings involving well-defined rules for the distribution of water given the water content as the only parameter accessible to experimental measurement.
- Experiments for qualitative and quantitative validation at the scale of the packing.

The capillary force between grains of different diameters is described in Section 2. We present DEM simulations of axial-compression tests in Section 3. The influence of water content and water distribution on the mechanical strength are investigated. The experiments are described in Section 4. Finally, in Section 5, we compare the numerical and experimental data and we discuss the assumptions used for the distribution of water.

2 Capillary cohesion between two grains of different diameters

At low water contents, the macroscopic cohesion of a granular material is ensured by the presence of pendular liquid bridges between grains. The liquid bridge between two spherical smooth grains of unequal diameters takes a complex axially symmetrical shape described by the Laplace-Young equation (Fig. 1):

$$\frac{\Delta p}{\sigma}\,(1+y'^2(x))^{3/2}+\frac{1+y'^2(x)}{y(x)}-y''(x)=0\,, \qquad (1)$$

where $\Delta p = p_{gas} - p_{liquid}$ is the pressure difference across the gas-liquid interface and σ is the surface tension of the liquid. The y-coordinate describes the profile of the liquid bridge along the common x-axis (Fig. 1). The resultant force in the presence of a liquid bridge can be calculated at the gorge [14,16], *i.e.* for the neck radius y_0 of the liquid bridge (Fig. 1). This force consists of contributions from the surface tension σ and the pressure difference Δp:

$$F = 2\,\pi\,y_0\,\sigma + \pi\,y_0^2\,\Delta p\,. \qquad (2)$$

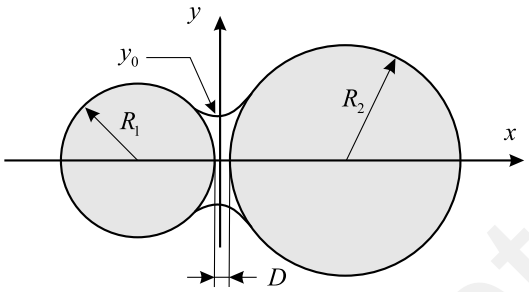

Fig. 1. Liquid bridge between two grains of unequal sizes.

Most expressions of the capillary force are based on assumptions of toroidal or parabolic shape of the liquid bridge and on the geometrical characteristics of the liquid bridge (such as the filling angle or the internal or external curvature radii) [20,21]. Apart from the difficulties involved in the measurement of these parameters, those expressions do not provide the evolution of the capillary force in the form of a force-displacement relationship accounting for the water content as a macroscopic quantity directly accessible to measurement. This point conducted us to search an explicit formulation of the capillary force as a function of the interstitial gap and the volume of the liquid bridge (these parameters being also accessible to local experimental measurements). For DEM simulations, we need the expression of the capillary force as an *explicit* function of local geometrical and physical parameters. The relevant parameters are the radii R_1 and R_2 of the grains (where R_2 is the radius of the larger grain), the inter-particle distance D, the volume V of the liquid bridge, the contact angle θ, and the liquid/air surface tension σ. The set of equations (1) and (2) is supplemented with geometrical equations describing the inter-particle distance, the volume of the liquid bridge and the boundary conditions at the solid-liquid-gas interface on the grains. We obtain a system of coupled non-linear equations describing the capillary force and the configuration of the doublet of grains. This system is numerically solved for several configurations of the doublet. Then, we seek a fitting form for this set of solutions. An appropriate fitting form is [22,23]

$$F = \pi\,\sigma\,\sqrt{R_1\,R_2}\,\left[c+\exp\left(a\,\frac{D}{R}+b\right)\right], \qquad (3)$$

where the coefficients a, b, and c are functions of the volume V of the liquid bridge, the contact angle θ and $R=\max(R_1,R_2)$:

$$\begin{aligned} a &= -1.1\,\left(\frac{V}{R^3}\right)^{-0.53}\,,\\ b &= \left(-0.148\ln\left(\frac{V}{R^3}\right)-0.96\right)\theta^2-0.0082\,\ln\left(\frac{V}{R^3}\right)+0.48,\\ c &= 0.0018\,\ln\left(\frac{V}{R^3}\right)+0.078. \end{aligned} \qquad (4)$$

Plots of this analytical form are shown in Figure 2 for several liquid-bridge volumes. For grains in contact

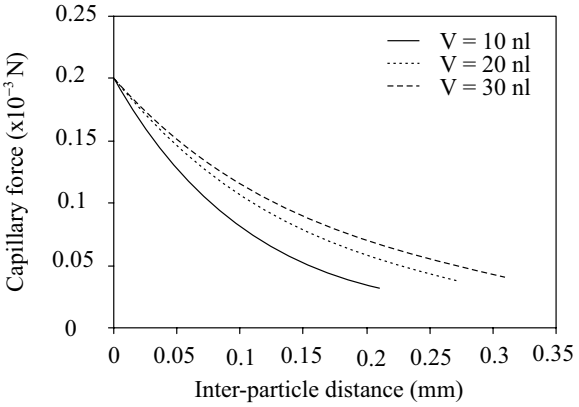

Fig. 2. Analytical estimate of the capillary force as a function of the inter-particle distance D for several volumes of liquid bridge V. The liquid bridge is assumed to be pure water ($\theta = 0$, $\sigma = 0.073\,\mathrm{N/m}$), the radii of grains are $R_1 = 0.4\,\mathrm{mm}$ and $R_2 = 0.65\,\mathrm{mm}$.

($D = 0$), the capillary force does not depend on V. We also see that the capillary force decreases for increasing inter-particle distance up to the rupture of the liquid bridge.

This rupture is determined according to a criterion expressing the rupture distance $D_{rupture}$ as a function of V and the contact angle [16]:

$$D_{rupture} = (1 + 0.5\,\theta)\,V^{1/3}. \tag{5}$$

We conducted experiments to measure the capillary force and rupture distance for several configurations of grain doublets [22,23]. The proposed fitting form is consistent with the experimental results for both the capillary force and the rupture distance. The analytical relations (Eqs. (3) and (4)) were also successfully compared to experimental results reported by Willett *et al.* [24].

3 Numerical simulations of axial-compression tests

We used a DEM code which was initially developed for the simulation of cohesive granular materials with cemented bonds between particles in two dimensions [25] and extended to three-dimensional polydisperse materials [26, 27]. The kinematics of the grains is determined by explicit integration of Newton's laws of motions according to the velocity Verlet scheme [28]. The grains are represented by spheres interacting by normal repulsion, Coulomb friction and capillary cohesion. The normal repulsion between particles is modeled by a linear elastic spring acting along the normal to the contact plane. The Coulomb friction law with viscous regularization at zero sliding velocity governs tangential forces. The capillary cohesion force between grains is a normal force described by the relations (3) and (4).

The implementation of capillary cohesion in a numerical code requires a method for the distribution of water in the packing. The total volume of water V_{liquid} is initially distributed according to the radii of the grain doublets. The liquid volume V_{ij} for a doublet composed of grains i and j is evaluated by the following rule:

$$V_{ij} = \frac{\tilde{V}_{ij}}{\sum_{k\in C}\tilde{V}_k} V_{liquid}\,, \tag{6}$$

where C denotes the set of capillary bonds and the indicative volume $\tilde{V}_{ij}$ is defined by

$$\tilde{V}_{ij} = R_i R_j (R_i + R_j). \tag{7}$$

According to this rule, larger grains acquire more water. During compression, this distribution evolves with the bond network: liquid bridges can be broken or created between neighbouring grains. The rupture of a liquid bridge occurs when the inter-particle distance exceeds the rupture distance (Eq. (5)). On the other hand, a new liquid bridge is created when two grains come into contact. The distribution of the total water content is renewed regularly, at the same time as the Verlet neighbourhood list [28], in order to keep the total volume of water V_{liquid} constant.

Axial-compression tests on polydisperse granular assemblies are simulated with a set of parameters given in Table 1 [23]. Parameters such as the contact stiffness, friction angle and wetting angle have been adapted to a packing of glass beads with well-known values [29,12,30, 13]. Initially, a packing composed of 8000 spherical grains with a given size distribution (Tab. 2) is generated by deposition under the action of gravity in a cylindrical box. We obtain a cylindrical sample with a diameter of 25 mm and a length of 17 mm (Fig. 3). The porosity is $n = 0.38$. This geometrical configuration of our numerical samples is identical to the experimental one considered in Section 4. The packing is then subjected to axial compression between two plates. The upper plate is moved downwards at a constant speed of 1 mm/s, while the lower plate is immobile. Axial-compression tests are performed for several values of water content (ratio of the total mass of water to the mass of the grains): $w = 0.5\%$, and from $w = 1\%$ to $w = 10\%$ by increments of 1%.

Table 1. Input parameters of numerical simulations.

Parameters	Values
Normal stiffness (N/m)	10^6
Inter-particle friction coefficient	0.3
Density of particles (kg/m^3)	2500
Time increment (s)	10^{-6}
Surface tension (N/m)	0.073
Contact angle (rad)	0

Table 2. Distribution of grain diameters in numerical simulations.

Diameter (mm)	0.8	0.9	1	1.1	1.2	1.3
Proportion (%)	10	20	20	20	20	10

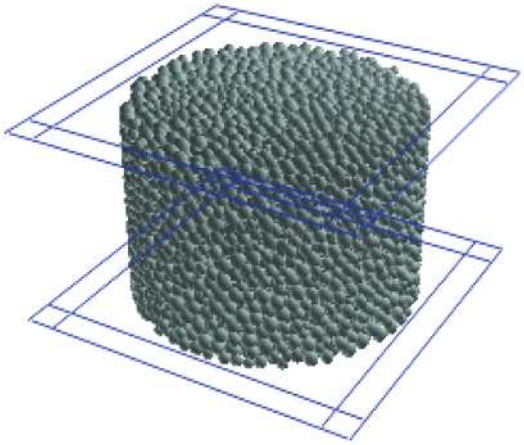

Fig. 3. Numerical granular assembly composed of 8000 spherical grains with diameters in the range from 0.8 mm to 1.3 mm.

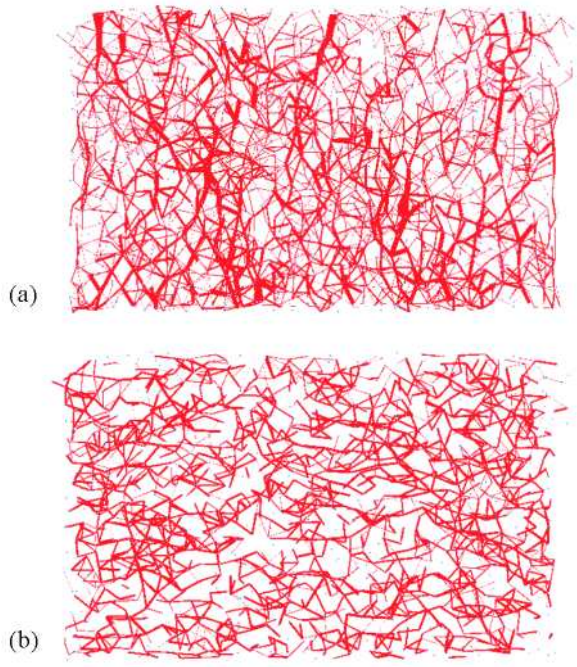

Fig. 4. Distribution of normal forces in a thin median vertical layer of the granular packing: (a) compressive forces, (b) tensile forces. The line thickness is proportional to the force.

We first consider the bond forces and particle displacements. Figure 4 shows the distribution of compressive and tensile forces in a thin median vertical layer. The thickness of the lines is proportional to the force. We see that a network of compressive forces appears preferentially along the vertical loading direction, whereas the tensile forces are mostly radial. This pronounced anisotropy is confirmed by Figure 5 that displays the polar diagrams of compressive and tensile forces along the vertical plane. The weak compressive forces (the range $0 < F_n < \langle F_n \rangle$, where $\langle F_n \rangle$ is the average normal force) have a nearly isotropic distribution. As Radjaï *et al.* showed [31], these weak forces prop strong force chains in the complementary "strong

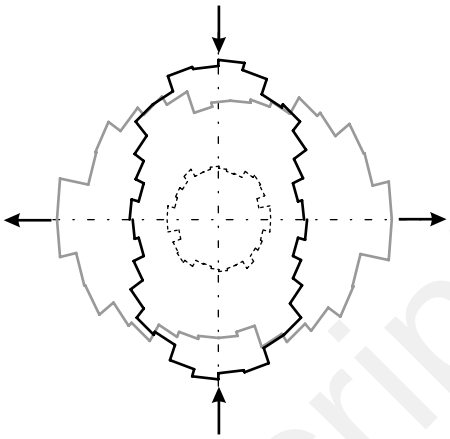

Fig. 5. Polar diagrams of strong (black solid line) and weak (dashed line) compressive forces, and tensile (gray solid line) forces along the vertical plane. The directions of extension and compression are represented by arrows.

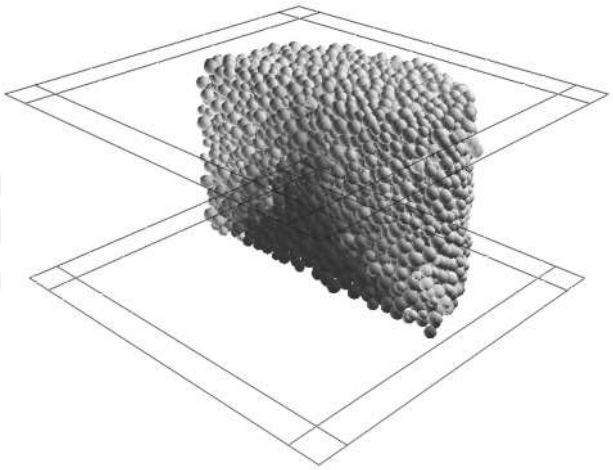

Fig. 6. Particle displacement field in a thin median vertical layer of the granular packing during the axial-compression test. The particle displacement is proportional to the clearness intensity. The gray levels represent the grain displacements ranging from zero displacement in dark to the largest displacement in white (about 1 mm).

network" (the range $F_n > \langle F_n \rangle$). The strong compressive forces form an anisotropic distribution with its longest axis oriented, as expected, in the loading direction. The tensile forces have an anisotropic distribution whose longest axis is perpendicular to that of compressive bonds, thus along the extension of the sample in the radial direction.

A snapshot of the particle displacement field is shown in Figure 6. We observe a well-defined discontinuity in particle motions. Two zones appear very clearly: on the one hand, the particles located in the upper and radial parts of the packing and, on the other hand, those located in the lower part. The large displacements of the particles in the first zone are due to the combined effects of gravity and the motion of the upper plate. The second zone, in which the particles are immobile, forms a cone supported at its base by the lower plate. The vertex angle is sharply

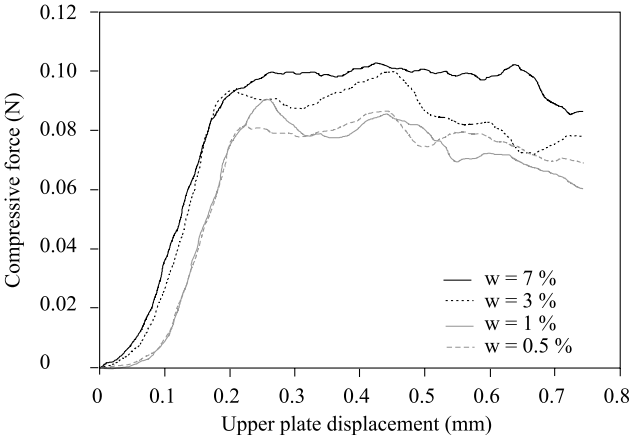

Fig. 7. Compressive axial force *versus* vertical displacement for $w = 0.5\%$, 1%, 3%, 7% in the numerical simulations.

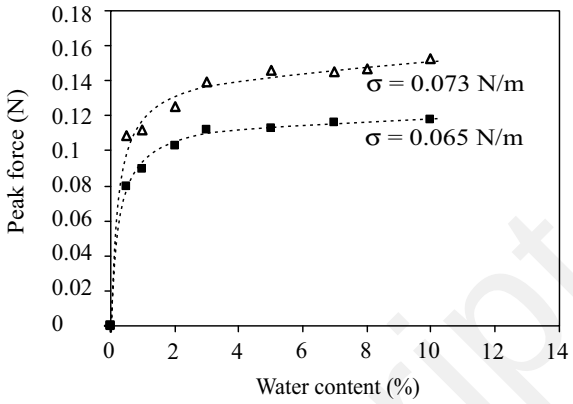

Fig. 8. Evolution of the peak force with water content for two different values of the surface tension. The dashed lines are drawn as a guide to the eyes.

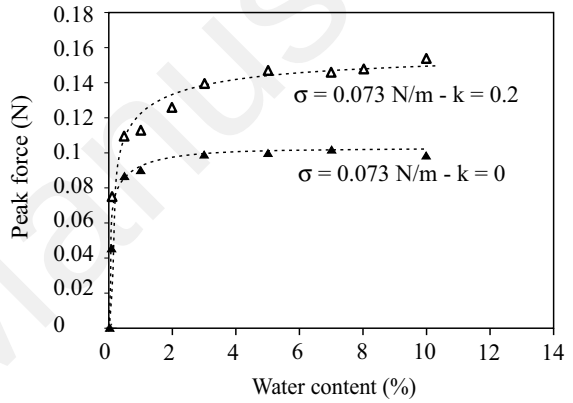

Fig. 9. Evolution of the peak force with water content for two protocols of water bridge formation; see text. The dashed lines are drawn as a guide to the eyes.

marked. This can be explained by the presence of capillary forces that allow high repose angles to be obtained in wet granular materials [1,32].

Figure 7 shows the evolution of the axial force as a function of the vertical displacement for four values of the water content $w = 0.5\%$, 1%, 3%, 7%. In all cases, the force increases (hardening) before declining (softening). The initial hardening is typical of granular media and it corresponds to the formation of strong contacts along the direction of compression. The overall dilation of the packing at the stress peak leads to a lower compactness and hence the increase of the mean inter-particle distance. As a result, the capillary forces decrease (Fig. 2) and the packing softens.

Figures 8 and 9 display peak forces as a function of water content from several simulations. The simulated water contents are below 10% in order to stay in the pendular state. This value is below the non-retaining water limit that corresponds to the value of the water content above which liquid water leaves the granular material due to gravity. In the dry case ($w = 0\%$), the rupture strength is zero, *i.e.* there is no cohesion and the granular assembly simply falls down under the action of its own weight. The peak force sharply increases with the water content, and seems to tend to a threshold value at high water contents.

These data represent the combined effect of several physical parameters involved in the expression of the capillary force according to equation (3). Let us analyze here, for example, the influence of the surface tension. Locally, the capillary force is directly proportional to the surface tension. As a result, we expect that the global strength of the material should increase with surface tension. This is what we observe in Figure 8 for two extreme cases: the pure water, for which $\sigma = 0.073\,\mathrm{N/m}$, and the case of water in the presence of impurities, for which surface tension is strongly reduced ($\sigma = 0.065\,\mathrm{N/m}$). This influence of surface tension on the strength of particle agglomerates is confirmed by experimental studies on glass beads [9].

The formation of the liquid bridges is a quite complex phenomenon. A fine description of the formation of a liquid bridge requires physical considerations and a thermodynamic framework [33,34]. In our simulations, a pragmatic approach, based on experimental observation, has allowed us to propose a simple geometrical criterion for the formation of a liquid bridge. This criterion is based on the inter-particle distance in comparison to the rupture criterion. Two cases can be considered:

- A liquid bridge can form between neighbouring grains which come into contact, that is for inter-particle distance equal to 0.
- A liquid bridge can form between two neighbouring grains as soon as the inter-particle distance is below a length $D_{formation}$ defined as a fraction k of the rupture distance:

$$D_{formation} = k\, D_{rupture}\,. \tag{8}$$

The parameter "k" allows us to adjust the distance below which a liquid bridge can be formed. For $k = 0$, the bridge can be formed only at the contact between two particles. On the other hand, $k = 1$ corresponds to the formation of a liquid bridge below a distance equal to the rupture distance. In between these two limits for $0 < k < 1$, the bridge formation distance is intermediary between these two limits. In all experiments performed, we realized that

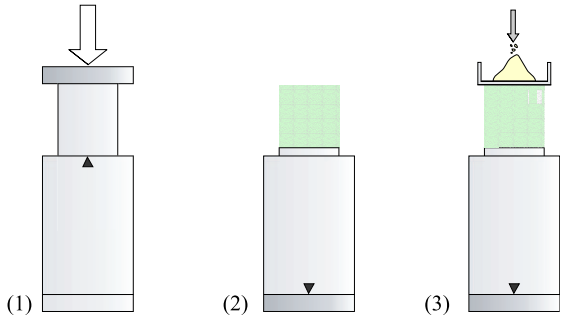

Fig. 10. Preparation of wet granular samples and axial-compression test: (1) the wet glass beads are compacted in a mould, (2) the sample is removed from the mould, (3) the sample is loaded incrementally until the rupture.

the value of k was close to 0 and would scarcely reach 0.2. This led us to consider the two extreme values of 0 and 0.2.

In Figure 9, we see that the peak force is higher in the second case. This observation can be explained by the increased number of liquid bridges. Indeed, at the beginning of the test, the number of liquid bridges for $k = 0.2$ is $\simeq 27\%$ above that for $k = 0$. This observation also underlines the importance of the number of liquid bridges on the mechanical behaviour of wet granular materials, as evoked by Soulié [23] and Richefeu [35]. The effects of structure, on the one hand, and those of the distribution of capillary forces, on the other hand, influence indeed strongly the mechanical behaviour of the granular material as underlined by the recent work by Bika *et al.* [36] and Fournier *et al.* [19].

4 Experimental approach

Experiments of axial compression were carried out on a reference material in view of comparison with numerical simulations. Experimental samples are composed of glass beads with diameters between 0.8 mm and 1.3 mm. The target water content for wet granular materials is obtained by mixing dry beads and the appropriate mass of demineralized water in a watertight box. The water content is controlled afterwards by differential weighting. The preparation of wet granular samples is done in a cylindrical metallic mould (Fig. 10). The wet glass beads are first poured into the mould and compacted by a piston. In a second time, the mould is turned over and the sample is slid out from the mould. The geometrical configuration of these experimental samples is identical to that in numerical simulations (Fig. 11).

Because of the characteristic weakness of capillary forces, the samples are so brittle that, in practice, they cannot be handled or displaced. For this reason, the sample preparation device is also used as support for the sample during the axial-compression test. The sample is loaded by adding dry sand into a plateau mounted on top of the sample (Fig. 10). The total load at the rupture of a sample is the peak force. In contrast to simulations, the sample is unstable at failure and the softening behaviour cannot be observed.

Fig. 11. Sample composed of glass beads prepared for axial-compression test.

Fig. 12. Features of the samples at the end of the axial-compression test: (a) at low water content $w = 1\%$, (b) at high water content $w = 10\%$.

The experiments were carried out for several water contents from $w = 1\%$ to $w = 12\%$. The influence of water content on the rupture is illustrated in Figure 12. For low water contents, the failure is sharp and it occurs at low force level; it looks like a brittle rupture. On the contrary, for high water contents, the deformation is progressive until full collapse occurs; the rupture appears to be ductile.

5 Results: comparison experiment-simulation

Plots of the peak force *versus* water content from experiments and numerical simulations are displayed in

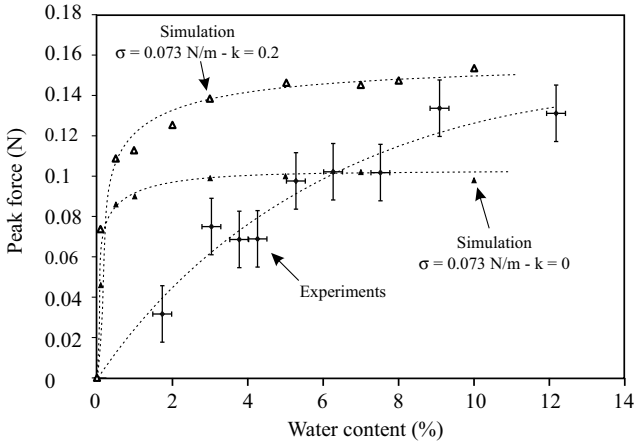

Fig. 13. Evolution of the peak force with water content in experiments and simulations. The dashed lines are drawn as a guide to the eyes.

Figure 13. The points represent the average data over five experiments, in exception to the dry case ($w = 0\%$) for which the experiment is unfeasible. The deviation bars represent the largest variability in the data. This dispersion is due to both the brittleness of the samples and the sample-to-sample fluctuations of the microstructure. Both in experiments and numerical simulations, the peak force increases with water content and the agreement is plausible in spite of discrepancies at low levels of the water content.

The uncertainty associated with the choice of various physical parameters can contribute to generate such discrepancies. The influence of surface tension was already discussed in Section 3. The value of the contact angle can also modify the magnitude of capillary forces. In our numerical simulations, the contact angle is set to zero, corresponding to pure water with the largest surface tension and thus the largest capillary force. The capillary force is reduced with an increase of the contact angle, an effect that might partly underlie the observed discrepancies. The contact angle can also present important hysteretic behaviour leading to a reduction of the capillary force [21]. Regarding the friction coefficient and normal stiffness, the values used in our numerical simulations are now almost classical for DEM simulations with glass beads and water (see, *e.g.*, [13]), and they are in agreement with experimental data. However, some degree of inaccuracy cannot be avoided, and the observed discrepancies might reasonably be attributed to the numerical values of such parameters.

The work by Halsey and Levine in 1998 [2], and more recently by Herminghaus [37], has shown the important effect of surface roughness on the behaviour of wet granular materials. Indeed, three regimes have been discerned for the capillary force between touching grains as a function of the liquid-bridge volume: an "asperity" regime, a "roughness" regime, and a "spherical" regime. Only this last regime is relevant to our study where the volume of the liquid bridges is large enough to circumvent the roughness effects in agreement with the assumption of smooth spherical grains. It is only in this configuration that the force at the contact point between two grains is maximal, the capillary forces corresponding to the "roughness" regime and, all the more, the "asperity" regime being considerably weaker. In numerical simulations, independently of the water content, it was the maximum capillary force at contact that was taken into account, leading to overestimation of cohesion between the grains as compared to experiments where the effects of roughness are present. These roughness effects might also be at the origin of observed differences between experimental and numerical data for low levels of the water content. Moreover, water is also partially "trapped" in the cavities of the rough surface, reducing thus the amount of water effectively mobilized for the formation of liquid bridges. Liquid droplets can also form due to the conjugated effects of the roughness and the wetting angle of the liquid. These droplets can be considered as a sort of water reservoir not directly mobilized for the creation of liquid bridges. The potential effects resulting from these two trapping mechanisms are all the more important as the water content is low. This might thus explain to some extent the low strength experimentally observed at very low levels of water content.

The rules governing the distribution of water inside the granular material also have a strong impact on the results. The way water is really distributed inside granular materials is poorly known. Even if the liquid is homogeneously distributed at a mesoscopic scale, the number of liquid bridges by particle remains a decisive factor [18,19]. Additional experimental work is necessary to improve our knowledge of the number and size of liquid bridges for various local configurations. In particular, it is necessary to consider a rather broad range of polydispersities, solid fractions and anisotropies of the granular packing as in real granular materials. We now discuss the relevance of our assumptions for water distribution.

One aspect of the problem concerns the number of liquid bridges per grain. Recent experimental data seem to show that the number of liquid bridges is only slightly higher than the number of contacts [18,19]. In our numerical simulations, the number of liquid bridges per grain is dependent on the parameters k. For $k > 0$, the number of liquid bridges per grain is overestimated in view of the above experimental results, and this might then explain the overestimation of the mechanical strength (Fig. 13). This means that for realistic simulations, the liquid should go only to contact points between grains.

The total volume of water is distributed in the sample using a rule based on the diameters of the partners of a capillary bridge (Eqs. (6) and (7)). One key parameter that governs the mechanical strength of the packing is the number of liquid bridges per unit volume. As shown in Figure 2, the volume of a liquid bridge have a weak influence onto the macroscopic behaviour. Consequently all kinds of homogeneous distribution of water, based on the same value of k (Eq. (8)), lead roughly to identical results. This is confirmed by several tests carried out using different rules [38]. A possible inhomogeneity of water distribution in the experimental sample should strongly

lower the macroscopic cohesion. Indeed, in regions with a deficit of liquid, capillary cohesion is reduced due to a lower number of bonds. On the other hand, in regions with a surplus of liquid, capillary cohesion is not necessarily enhanced, because the volume of liquid has little impact on the capillary force at low inter-particle distances (Sect. 2). In other words, the presence of local aggregates reduces the amount of water available for the formation of otherwise more liquid bridges [19]. Despite our precautions in the process of sample preparation, some degree of inhomogeneity should persist in our samples. This is particularly obvious at low water contents, where very small liquid volume bridges are unstable. For all these reasons, it is plausible to attribute the higher mechanical strength in numerical simulations at lower water contents to the fact that our granular samples are more homogeneous in simulations than in experiments.

It is also important to remark that the number of liquid bridges per unit volume is inversely proportional to the cube of the mean particle diameter. Since the mechanical strength is defined as the peak force per unit area, the mechanical strength for a given volume of water and grains increases in proportion to the inverse of the mean grain size. For the same reason, the mechanical strength declines with the dilation of the packing (Sect. 2).

6 Conclusion

We studied the influence of capillary cohesion on the mechanical strength of wet polydisperse granular materials both by experiments and numerical simulations.

The capillary force between two grains of unequal sizes was described by an explicit expression as a function of the physical and geometrical characteristics of the grains. This expression was used in a three-dimensional DEM algorithm in order to simulate axial compression of polydisperse granular assemblies for several levels of the water contents. As a function of the vertical displacement, the force increases up to a peak (hardening), before declining (softening). We also conducted experiments of axial compression of wet packings of glass beads in nearly the same conditions as in numerical simulations. The experimental and numerical data were in good agreement in terms of the mechanical strength as a function of water content: the peak force increases with water content.

We analyzed the crucial role of the distribution of liquid bridges inside the granular mass. The importance of the density of liquid bridges and the role of their inhomogeneities were discussed. The development of appropriate experimental procedures in order to access detailed local information together with numerical simulations appears as a key point for a better understanding of the mechanical behaviour of wet granular materials.

We gratefully thank J.-Y. Delenne, J.-J. Moreau, F. Radjaï and V. Richefeu for interesting discussions.

References

1. D.J. Hornbaker, R. Albert, I. Albert, A.L. Barabási, P. Schiffer, Nature **387**, 765 (1997).
2. T.C. Halsey, A.J. Levine, Phys. Rev. Lett. **80**, 3141 (1998).
3. J.K. Mitchell, *Fundamentals of Soil Behavior*, 2nd ed. (Wiley Inter Science, 1993).
4. S.M. Iveson, J.D. Litster, K. Hapgood, B.J. Ennis, Powder Technol. **117**, 3 (2001).
5. A. Nokhodchi, Pharm. Technol. **29**, 46 (2005).
6. S.M. Iveson, J.D. Litster, B.J. Ennis, Powder Technol. **88**, 15 (1996).
7. P. Pierrat, H.S. Caram, Powder Technol. **91**, 83 (1997).
8. T.H. Kim, C. Hwang, Eng. Geol. **69**, 233 (2003).
9. X. Rondeau, C. Affolter, L. Komunjer, D. Clausse, P. Guigon, Powder Technol. **130**, 124 (2003).
10. G. Lian, C. Thornton, M.J. Adams, Chem. Eng. Sci. **53**, 3381 (1998).
11. C. Thornton, M.T. Ciomocos, M.J. Adams, Powder Technol. **140**, 258 (2004).
12. T. Mikami, H. Kamiya, M. Horio, Chem. Eng. Sci. **53**, 1927 (1998).
13. T. Gröger, U. Tüzün, D.M. Heyes, Powder Technol. **133**, 203 (2003).
14. K. Hotta, K. Takeda, K. Iionya, Powder Technol. **10**, 231 (1974).
15. J. Israelachvili, *Intermolecular and Surface Forces*, 2nd ed. (Academic Press, Londres, 1992).
16. G. Lian, C. Thornton, M.J. Adams, J. Colloid Interface Sci. **161**, 138 (1993).
17. O. Pitois, P. Moucheront, X. Chateau, J. Colloid Interface Sci. **231**, 26 (2000).
18. M.M. Kohonen, D. Geromichalos, M. Scheel, C. Schier, S. Herminghaus, Physica A **339**, 7 (2004).
19. Z. Fournier, D. Geromichalos, S. Herminghaus, M.M. Kohonen, F. Mugele, M. Scheel, M. Schulz, B. Schulz, C. Schier, R. Seemann *et al.*, J. Phys.: Condens. Matter **17**, S477 (2005).
20. R.J. Fairbrother, S.J.R. Simons, Part. Part. Syst. Charact. **15**, 16 (1998).
21. X. Pepin, S.J.R. Simons, S. Blanchon, D. Rossetti, G. Couarraze, Powder Technol. **117**, 123 (2001).
22. F. Soulié, F. Cherblanc, M.S. El Youssoufi, C. Saix, Int. J. Numer. Anal. Methods Geomech. **30**, 213 (2006).
23. F. Soulié, PhD Thesis, Université Montpellier II (2005).
24. C.D. Willett, M.J. Adams, S.A. Johnson, J.P.K. Seville, Langmuir **16**, 9396 (2000).
25. J.Y. Delenne, M.S. El Youssoufi, F. Cherblanc, J.C. Bénet, Int. J. Numer. Anal. Methods Geomech. **28**, 1577 (2004).
26. V. Richefeu, M.S. El Youssoufi, R. Peyroux, C. Bohatier, *Frictional Contact and Cohesion Laws for Casagrande's Shear Test on Granular Materials by 3D DEM - Comparison with Experiments*, in *Powders and Grains*, edited by R. García-Rojo, H.J. Herrmann, S. McNamara (Taylor & Francis Group, London, 2005) pp. 509-512.
27. F. Soulié, M.S. El Youssoufi, F. Cherblanc, C. Saix, *Influence of Water Content on the Mechanical Behavior of Granular Assemblies*, in *Powders and Grains*, edited by R. García-Rojo, H. Herrmann, S. McNamara (Taylor & Francis Group, London, 2005) pp. 599-603.
28. M.P. Allen, D.J. Tildesley, *Computer Simulation of Liquids* (Oxford University Press, Oxford, 1987).

29. C. Thornton, K. Yin, M. Adams, J. Phys. D: Appl. Phys. **29**, 424 (1996).
30. C. Thornton, S.J. Antony, Powder Technol. **109**, 179 (2000).
31. F. Radjaï, D.E. Wolf, M. Jean, J.J. Moreau, Phys. Rev. Lett. **80**, 61 (1998).
32. P. Tegzes, R. Albert, M. Paskvan, A.L. Barabási, T. Vicsek, P. Schiffer, Phys. Rev. E **60**, 5823 (1999).
33. H. Christenson, Phys. Rev. Lett. **73**, 1821 (1994).
34. J. Crassous, E. Charlaix, H. Gayvallet, J.L. Loubet, Langmuir **9**, 1995 (1993).
35. V. Richefeu, PhD Thesis, Université Montpellier II (2005).
36. D. Bika, M. Gentzler, J. Michaels, Powder Technol. **117**, 98 (2001).
37. S. Herminghaus, Adv. Phys. **54**, 221 (2005).
38. V. Richefeu, Tech. rep., Laboratoire de Mécanique et Génie Civil, UMR CNRS-UM2 5508 (2005).